CRYSTALLOGRAPHY REPORTS, 2025, Vol. 70, No. 1, pp. 80–85

SURFACE, THIN FILMS

CESIUM HYDROSULFATE PHOSPHATE CRYSTALS: CONDUCTIVITY AND REAL STRUCTURE AT INCREASING TEMPERATURE

© 2025 R. V. Gainutdinov[a], A. L. Tolstikhina[a,*], I. P. Makarova[a], S. Leesment[b], and V. A. Komornikov[a]

[a] *Shubnikov Institute of Crystallography, Kurchatov Complex of Crystallography and Photonics, National Research Centre "Kurchatov Institute", Moscow, Russia*

[b] *LLC "Xillect", Moscow, Russia*

**e-mail: alla@crys.ras.ru*

Received November 13, 2024
Revised November 13, 2024
Accepted November 18, 2024

Abstract. Superprotonic crystals $Cs_3(HSO_4)_2(H_2PO_4)$ and $Cs_4(HSO_4)_3(H_2PO_4)$ have been investigated by conducting atomic force microscopy at increasing temperature. Local volt-ampere characteristics have been measured and an increase in conductivity at 413-453 K for $Cs_3(HSO_4)_2(H_2PO_4)$ and $Cs_4(HSO_4)_3(H_2PO_4)$ by two and three orders of magnitude, respectively, has been recorded. Differences in the conductive characteristics of crystals of different compositions in the vicinity of the phase transition are shown. Information on topographic and electrical features of crystalline phases before and after exposure to temperature and electric fields has been obtained. The influence of external factors on the stability of the surface microstructure is evaluated. Possible mechanisms of structural-phase transformations of isostructural compounds with different ratio of sulfate and phosphate groups are discussed.

DOI: 10.31857/S00234761250111e9

INTRODUCTION

Crystals of cesium hydrosulfate $CsHSO_4$ (**CHS**) and cesium dihydrogen phosphate CsH_2PO_4 (**CDP**) are actively studied in connection with the prospects of their use in electrochemical devices, including fuel cells, providing direct conversion of chemical energy into electrical energy in the temperature range of 300–500 K [1–9]. Despite the accumulated experimental material for a large number of superprotonic crystals, there are still significant disagreements in the interpretation of the relationship between the structure and properties of superprotonic phases, including for complex compounds of cesium hydrosulfate phosphates.

The effect of anomalously high conductivity in mixed compounds of the $CsHSO_4$–CsH_2PO_4 system was explained, for example, by the removal of crystallization water [10, 11]. According to [10, 11], the β-$Cs_3(HSO_4)_2[H_{2-x}(P_{1-x}, S_x)O_4)]$ ($x \sim 0.5$) compound does not have a superprotonic conducting phase as such, and the endothermic effect observed at 398 K is due exclusively to dehydration processes that occur on the crystal surface and contribute to high protonic conductivity above this temperature. It should be mentioned that in [12], surface conductivity anomalies in CHS at a certain characteristic temperature of 395 K were associated with phase transitions in the surface layers, but not with adsorption ($T > 373$ K) and desorption ($T \approx 373$ K) of water on the crystal surface.

According to X-ray powder diffractometry data, the transition from the low-temperature to the high-temperature conducting phase in $Cs_3(HSO_4)_2(H_2PO_4)$ at 411 K and $Cs_4(HSO_4)_3(H_2PO_4)$ at 409 K occurs through separation into constituent phases similar in their parameters to CHS and CDP, and upon cooling, the previous monoclinic crystal structure is stabilized [13].

Clearly, additional data on the behavior of the system near the phase transition with the use of techniques with nanometer spatial resolution are required to describe the structure of superprotonic phases and the mechanisms of phase transformations. Atomic force microscopy (**AFM**) with the possibility of visual non-destructive testing of the surface and the availability of precise methods for local determination of various physical parameters can be effectively used to study superprotonic compounds [3, 14–17].

In this paper, we carried out a microscopic study of the surface and conductive properties of crystalline samples of $Cs_3(HSO_4)_2(H_2PO_4)$ and $Cs_4(HSO_4)_3(H_2PO_4)$ at temperatures near the phase transition and at room temperature after cooling, aimed at identifying fine details of structural rearrangements in the bulk and surface layers. Evaluation of the real role of dehydration processes closely related to the surface state, formation of highly conductive phases, analysis and comparison of local electrical characteristics of isostructural crystalline compounds were in the center of attention. It was important to analyze the influence of external influences on the surface characteristics of materials on a microscale.

OBTAINING AND CHARACTERIZING CRYSTALLINE SAMPLES

$Cs_3(HSO_4)_2(H_2PO_4)$ and $Cs_4(HSO_4)_3(H_2PO_4)$ were grown from aqueous solutions by the method of controlled temperature reduction of a saturated solution [18]. At room temperature, the crystals have a monoclinic structure with space group $C2/c$ [13]. Samples for AFM were obtained by fresh cleavage perpendicular to the a-axis from single-crystal samples collected using a Nikon SMZ1270 stereomicroscope with magnification up to 80×. The usual shape of the crystals can be characterized as plates with a uniform horizontal layering of the structure or close to it (with orientation perpendicular to the a-axis), which is clearly visible at the micro- and macrolevel [19].

EXPERIMENTAL SETUP AND MEASUREMENT TECHNIQUES

Temperature measurements of local physical properties of crystals were performed on an NTEGRA Prima atomic force microscope (NT-MDT Spectrum Instruments, Zelenograd) in the clean zone conditions of the TRACKPORE ROOM-05 control and measuring complex (cleanliness class 5 ISO (100), the accuracy of maintaining the temperature (T) of the air in the clean zone in the range of 298 ± 5 K was ± 0.05 K, at a relative air humidity of 35–70 % the accuracy was ± 1 %). The silicon cantilever (HA_FM, beam A, Kapela LLC, Zelenograd) coated with Pt had the following characteristics: resonance frequency f = 114 kHz, stiffness k = 6 N/m, tip curvature radius R < 35 nm. Local current-voltage characteristics (**CVC**) were measured in the voltage range from –10 to +10 V. The surface relief of the samples was studied in intermittent contact mode using cantilevers of the same brand.

The surface potential distribution was recorded using the Kelvin scanning microscopy (**KSM**) method in contactless mode based on the compensation principle (the constant component of the applied voltage U_{DC} was selected so that cantilever oscillations at the frequency ω, caused by the variable voltage component, were absent). The potential measurements were performed in the amplitude modulation mode. An alternating current bias voltage U_{AC} = 2 V with a frequency of 114 kHz was applied to the sample.

DISCUSSION OF RESULTS

Temperature dependence of local conductivity of crystals. To study the temperature dependence of electrical conductivity on the composition of the compounds, local CVC were measured along the a axis with stepwise heating of the samples to 453 K (Fig. 1). The presented graphs of the $I(U)$ dependences of the probe-sample contact for the compositions $Cs_3(HSO_4)_2(H_2PO_4)$ (Fig. 1a) and $Cs_4(HSO_4)_3(H_2PO_4)$ (Fig. 1b) were obtained for a static position of the probe when applying a positive bias voltage from 0 to +5 V. It is evident that the CVC of both compounds exhibit common features. In the temperature range of 300–393 K, the most characteristic is the CVC, which has a close to linear dependence of the current on voltage, which indicates a predominantly ohmic conductivity mechanism. At 453 K, the type of CVC changes significantly – in the section U > +2 V, the current increases sharply, which indicates transitions to a high-temperature phase with high ionic conductivity. At 293 K, the conductivity $\sigma_{DC} = 9.43 \times 10^{-2}$ $\Omega^{-1}\cdot cm^{-1}$ for $Cs_3(HSO_4)_2(H_2PO_4)$, $\sigma_{DC} = 3.34 \times 10^{-2}$ $\Omega^{-1}\cdot cm^{-1}$ for $Cs_4(HSO_4)_3(H_2PO_4)$. At 453 K (U = + 4V) $\sigma_{DC} = 1.34 \times 10^{1}$ $\Omega^{-1}\cdot cm^{-1}$ for the composition $Cs_3(HSO_4)_2(H_2PO_4)$, $\sigma_{DC} = 2.77 \times 10^{1}$ $\Omega^{-1}\cdot cm^{-1}$ for

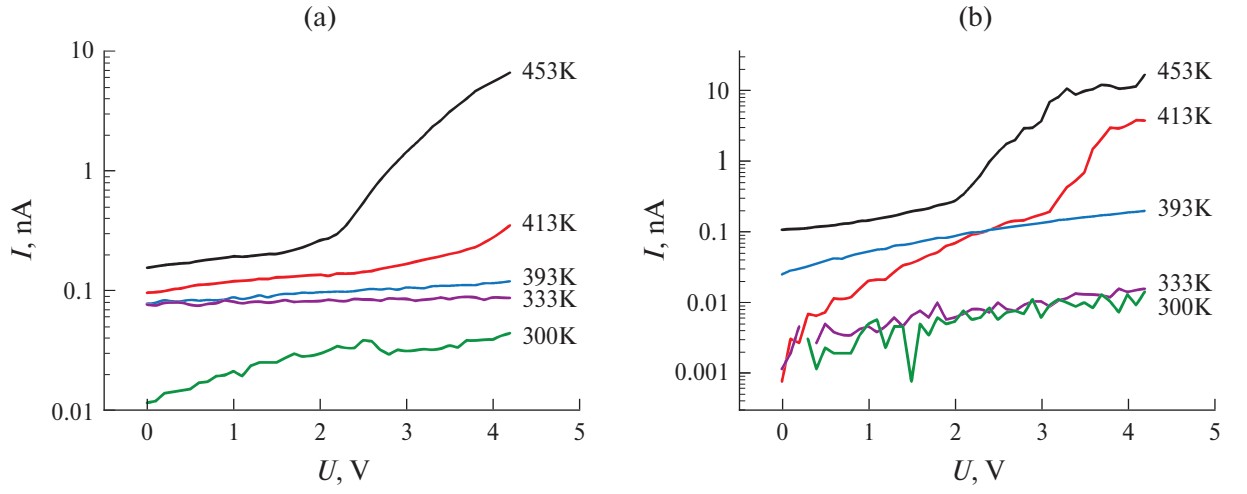

Fig. 1. Local CVCs of $Cs_3(HSO_4)_2(H_2PO_4)$ (a) and $Cs_4(HSO_4)_3(H_2PO_4)$ (b) samples, recorded along the a axis under atmospheric conditions at 300, 333, 393, 413, 453 K.

the composition $Cs_4(HSO_4)_3(H_2PO_4)$, which are 2 and 3 orders of magnitude higher, respectively, than in the low-temperature state. In the temperature range of 413–453 K, the $I(U)$ dependences show an increase in conductivity for both samples. This region corresponds to the first stage of thermal dissociation of mixed compounds, when the crystal transforms into a mixture of high-temperature tetragonal and cubic superprotonic phases [13].

Let us consider in detail the characteristics of the samples at a certain average temperature of 393 K, which indicate a different nature of conductivity near the phase transition (Fig. 2). The CVC of $Cs_3(HSO_4)_2(H_2PO_4)$ crystals has a diode character – a large unidirectional current is formed at a voltage on the sample starting from $U = +5$ V (Fig. 2). The same diode character of the CVC at a positive voltage on the sample was observed in proton-conducting membranes based on Nafion, when positive charge carriers from the sample are attracted to the AFM probe and the current flow between the probe and the surface leads to depletion of local conductivity [20]. The CVC of $Cs_4(HSO_4)_3(H_2PO_4)$ crystals has a linear character at positive and negative voltage on the sample if electron conductivity is predominant (Fig. 2). That is, when heating compounds in the vicinity of phase transitions, the simultaneous presence of ionic and electronic conductivity is observed, but the proportion of electronic conductivity in $Cs_4(HSO_4)_3(H_2PO_4)$ is slightly higher than in $Cs_3(HSO_4)_2(H_2PO_4)$.

At this stage of the work, as a result of measuring CVC, we have confirmed the increase in conductivity by 2–3 orders of magnitude during structural phase transitions in cesium hydrosulfate phosphate crystals, associated with the motion of protons. Similar conclusions were made during AFM measurements of CVC of CHS crystals at 413 K [14]. To obtain fundamental characteristics of electrical conductivity as a function of temperature, additional studies of complex compounds are required. As is known, probe measurements in the contact mode at phase transition temperatures are associated with difficulties due to the superplasticity of the superprotonic phase of crystals [14]. When approaching the phase transition temperature, significant distortions and disturbances occur in crystals, and the degree of defectiveness of samples increases. Structural defects, proton movements on hydrogen bonds, reorientation of sulfate and phosphate groups, as well as migration of heavier ions act as charge carriers and contribute to electrical conductivity.

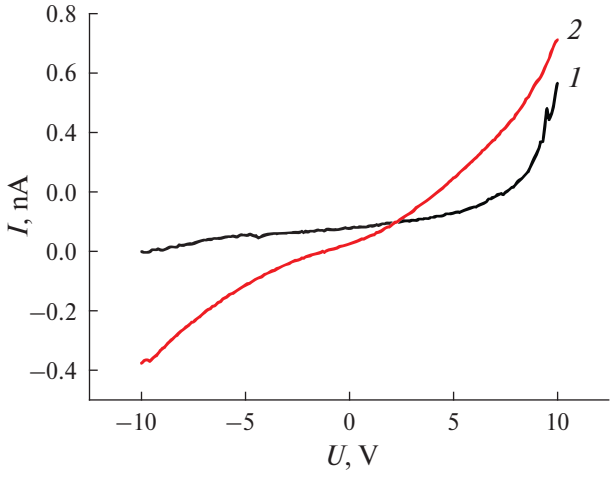

Fig. 2. Local CVCs of samples recorded along the *a* axis at 393 K: a – $Cs_3(HSO_4)_2(H_2PO_4)$, b – $Cs_4(HSO_4)_3(H_2PO_4)$.

Morphology of crystalline surfaces and surface potential. To clarify the microscopic mechanisms of structural changes, the crystals were studied after a single cycle – heating to 393 K and cooling to room temperature. During heat treatment, the crystal structure was rebuilt without changing the original external shape of the samples. In the images of the surface oriented perpendicular to the *a* axis, one can see how the crystals are broken down into individual submicroscopic blocks and crystalline aggregates (Fig. 3). For example, in the $Cs_3(HSO_4)_2(H_2PO_4)$ sample, areas of a new phase several microns in size with a mosaic structure are formed (Figs. 3a, 3b). The length of the blocks is 350–2100 nm (average value 840 nm), the width is 300–1500 nm (average value 540 nm), the height difference is 5500 nm (Fig. 3b). The surface potential is distributed uniformly within individual blocks, excluding the boundaries between them (Fig. 3c). $Cs_4(HSO_4)_3(H_2PO_4)$ is characterized by plate-shaped microblocks with different spatial orientations and smaller crystallites (Fig. 3d, 3e), and individual twin layers can be traced (Fig. 3d). Between the blocks and surface crystallites there are channels and voids up to several microns deep (Fig. 3a, 3b, 3d, 3e). In other words, thermal action leads to the development of a block structure and disruption of the continuity of the surface layers of the crystal. A feature of the spatial structural organization of monoclinic phases is the morphologically stable plate-shaped form of the block-crystallites after recrystallization.

The surface of the monoclinic phases formed after heating (after recrystallization) is positively charged: the surface electrostatic potential U_{CPD} is 65–200 mV for $Cs_3(HSO_4)_2(H_2PO_4)$ samples, 20–60 mV for $Cs_4(HSO_4)_3(H_2PO_4)$ samples. For single crystals, the potential value was slightly higher – 95–300 mV. It can be concluded that during structural rearrangement in the volume, the surface potential does not change sign, i.e. the electrical characteristics and, apparently, the acid-base properties of the surface of complex compounds change little.

One of the necessary conditions for understanding structural changes is to measure the structural response to an external effect, such as an electric field. Experiments have shown that in the fields of an AFM probe coated with platinum, which catalyzes dehydration reactions, no channels for water to exit the volume or nanobubbles

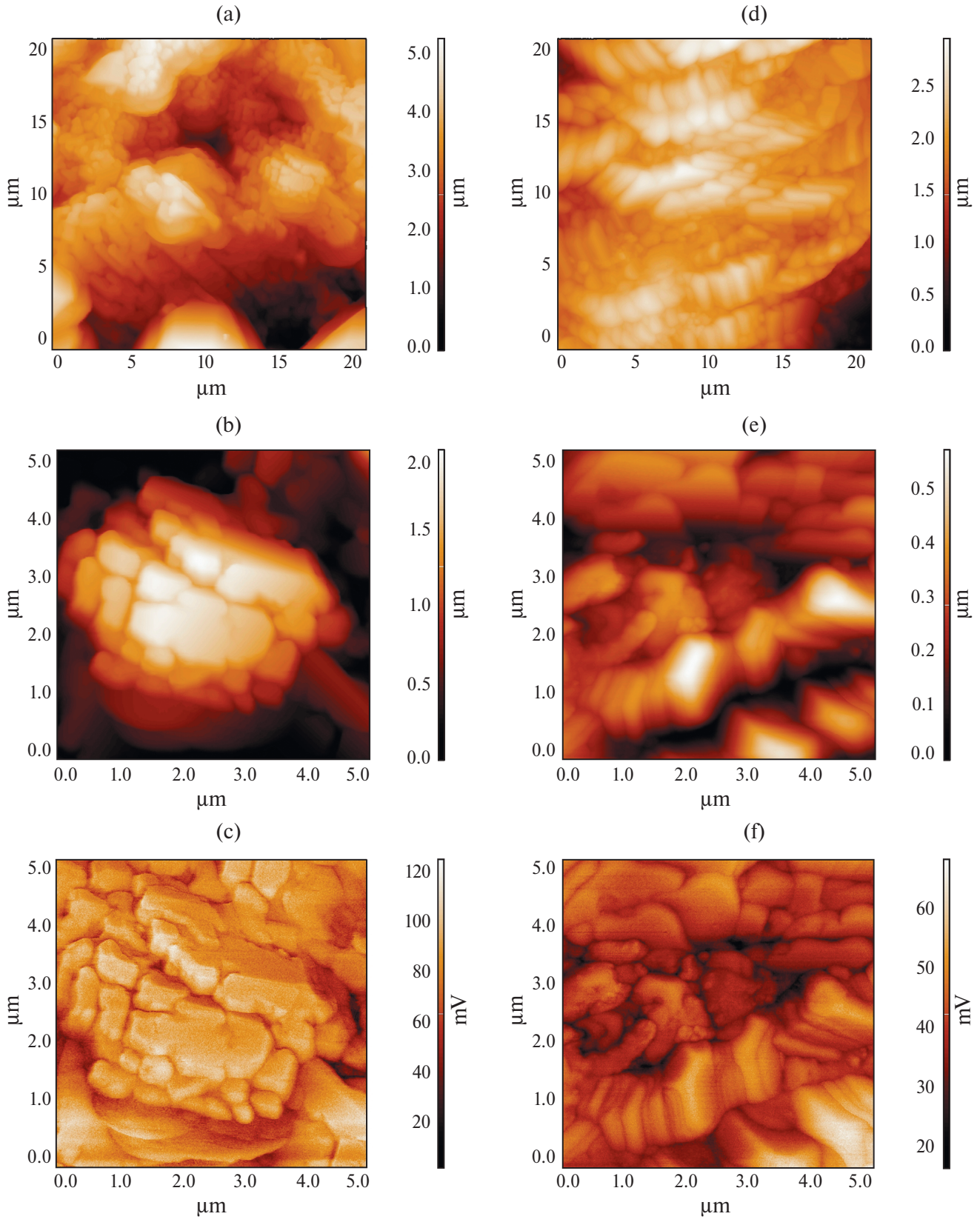

Fig. 3. AFM images of the surface of samples at 296 K, preheated to 393 K: a, b, c – $Cs_3(HSO_4)_2(H_2PO_4)$, d, e, f – $Cs_4(HSO_4)_3(H_2PO_4)$. Topography (a, b, d, e), surface potential (c, f). The image plane is perpendicular to the *a* axis.

are formed, as, for example, in superprotonic crystals of acidic salts of potassium ammonium sulfate [21]. The surface is weakly susceptible to the effects of atmospheric moisture and electric fields. The $Cs_3(HSO_4)_2(H_2PO_4)$ crystal does not respond to voltage up to 40 V for 10 s (higher – it switches under the probe). The $Cs_4(HSO_4)_3(H_2PO_4)$ sample is less stable and switches already at 15 V and is destroyed at 25 V. For comparison, note that the hydrogen-containing triglycine sulfate crystal is destroyed under the probe already at 10 V.

It should be noted that the surface of monoclinic crystals perpendicular to the *a*-axis turned out to be most susceptible to changes and rearrangements, since its formation is already associated with the rupture of disordered hydrogen bonds connecting SO_4 groups, which, due to the participation of only two oxygen atoms in these hydrogen bonds, can perform reorientation vibrations [22]. Crystals $Cs_3(HSO_4)_2(H_2PO_4)$ and $Cs_4(HSO_4)_3(H_2PO_4)$ have physical properties that correlate with the ratio of SO_4 and PO_4 groups in the unit cell and with some orientational freedom of SO_4 groups. At the same time, the results of the study of the real structure indicate that violations of the homogeneity of the crystal structure and the types of defects do not remain constant during heating and cooling of the samples and can change depending on the crystallization conditions. Electrophysical, polarization and other physicochemical properties of superprotonic compounds cannot be considered independently of their real structure, including the surface.

CONCLUSION

Microscopic study of the surface and temperature dependence of the conductive properties of complex crystalline compounds contributes to a deeper understanding of the structural aspects of changes in their functional properties. The availability of accurate data on the atomic structure of monoclinic crystals $Cs_3(HSO_4)_2(H_2PO_4)$ and $Cs_4(HSO_4)_3(H_2PO_4)$ served as the basis for choosing the most informative crystallographic plane, namely, perpendicular to the *a*-axis, and studying the local properties and morphology of the corresponding surface using *in situ* and *ex situ* AFM methods with nanoscale spatial resolution. A comparative study of two isostructural compounds of cesium hydrosulfate phosphates revealed the presence of correlations between their properties and structure at the level of atomic and nanometer scales. The AFM methods established the formation of a non-uniform defect structure of the surface layers already at the approach to the phase transition, as well as such material characteristics as the positive electric potential of the surface of monoclinic phases of different degrees of crystallinity, relative resistance to external electric fields and atmospheric humidity.

An important result of this stage of the work was the confirmation of the formation of high-temperature conducting phases in the studied compounds by the AFM method. For the first time, local current-voltage characteristics along the *a* axis were measured for $Cs_3(HSO_4)_2(H_2PO_4)$ and $Cs_4(HSO_4)_3(H_2PO_4)$ crystals, and an increase in conductivity by 2 and 3 orders of magnitude, respectively, was recorded at 413–453 K. Common features and differences in the nature of local conductivity at 393 K for samples of different compositions, associated with the rearrangements of both the atomic and real structure of crystals during phase transitions, are shown.

FUNDING

The work was carried out within the framework of the State assignment of the National Research Center "Kurchatov Institute".

CONFLICT OF INTERESTS

The authors have no conflicts of interest.

REFERENCES

1. *Haile S.M., Boysen D.A., Chisholm C.R.I., Merle R.B.* // Nature. 2001. V. 410. P. 910. https://doi.org/10.1038/35073536
2. *Pawlaczyk Cz., Pawłowski A., Połomska M. et al.* // Phase Transitions. 2010. V. 83. P. 854. http://dx.doi.org/10.1080/01411594.2010.509159
3. *Louie M.W., Hightower A., Haile S.M.* // ACS Nano. 2010. V. 4. No. 5. P. 2811.
4. *Paschos O., Kunze J., Stimming U., Maglia F.* // J. Phys.: Condens. Matter. 2011. V. 23. P. 234110. http://dx.doi.org/10.1088/0953-8984/23/23/234110
5. *Ponomareva V., Lavrova G.* // Solid State Electrochem. 2011. V. 15. P. 213. https://doi.org/10.1007/s10008-010-1227-1
6. *Dupuis A.-C.* // Progress in Materials Science. 2011. V. 56. P. 289. http://dx.doi.org/10.1016/j.pmatsci.2010.11.001
7. *Mohammad N., Mohamad A.B., Kadhum A.A.H., Loh K.S.* // J. Power Sources. 2016. V. 322. P. 77. https://doi.org/10.1016/j.jpowsour.2016.05.021
8. *Aili D., Gao Y., Han J., Li Q.* // Solid State Ionics. 2017. V. 306. P. 13. http://dx.doi.org/10.1016/j.ssi.2017.03.012
9. *Colomban P.* // Solid State Ionics. 2019. V. 334. P. 125. https://www.researchgate.net/publication/331249475
10. *Ortiz E., Vargas R.A., Tróchez J.C. et al.* // J. Phys. Status Solidi. C. 2007. V. 4. No. 11. P. 4070. https://doi.org/10.1002/pssc.200675933
11. *Ortiz E., Pin˜eres I., Leo´n C.* // J. Therm. Anal. Calorim. 2016. V. 126. P. 407. https://doi.org/10.1007/s10973-016-5474-y
12. *Baranov A.I., Sinitsyn V.V., Ponyatovsky E.G., et al.* // Letters to JETP. 1986. V. 44. No. 44. P. 186.

13. *Mikheykin A.S., Chernyshov D.Yu., Makarova I.P. et al.* // Solid State Ionics. 2017. V. 305. P. 30. https://doi.org/10.1016/j.ssi.2017.04.017
14. *Papandrew B., Li Q., Okatan M.B. et al.* // Nanoscale. 2015. V. 7. P. 20089. https://doi.org/10.1039/c5nr04809e
15. *Kalinin S., Dyck O., Balke N. et al.* // ACS Nano. 2019. V. 13. No. 9. P. 9735. https://doi.org/10.1021/acsnano.9b02687
16. *Kempaiah R., Vasudevamurthy G., Subramanian A.* // Nano Energy. 2019. P. 103925. https://doi.org/10.1016/j.nanoen.2019.103925
17. *Gainutdinov R.V., Tolstikhina A.L., Selezneva E.V., Makarova I.P.* // JTF. 2020. No. 11. P. 1843. https://doi.org/10.21883/JTF.2020.11.49972.116-20
18. *Komornikov V.A., Grebenev V.V., Makarova I.P. et al.* // Crystallography. 2016. V. 61. No. 4. P. 645. https://doi.org/10.1134/S1063774516040106
19. *Gainutdinov R.V., Tolstikhina A.L., Selezneva E.V. et al.* // Crystallography. 2024. V. 69. No. 3. P. 470. https://doi.org/10.31857/S0023476124030129
20. *Ankudinov A.V., Gushchina E.V., S.A. Gurevich S.A. et al.* // International scientific journal "Alternative energy and ecology". 2008. No. 10 (66). P. 30.
21. *Gainutdinov R.V., Tolstikhina A.L., Selezneva E.V. et al.* // Crystallography. 2023. V. 68. No. 2. P. 290. https://doi.org/10.31857/S0023476123020066
22. *Makarova I.P., Isakova N.N., Kalyukanov A.I. et al.* // Acta Cryst. B. 2024. V. 80. P. 201. https://doi.org/10.1107/s2052520624003470 Q2